Reynolds stresses and mean fields generated by pure waves: applications to shear flows and convection in a rotating shell

E. PLAUT[1], Y. LEBRANCHU[1], R. SIMITEV[2] AND F. H. BUSSE[3]

[1]LEMTA, Nancy-Université & CNRS, 2 av. Forêt de Haye, 54516 Vandoeuvre cedex, France
[2]Department of Mathematics, University of Glasgow, Glasgow, G12 8QW, UK
[3]Institute of Physics, University of Bayreuth, 95440 Bayreuth, Germany

A general reformulation of the Reynolds stresses created by two-dimensional waves breaking a translational or a rotational invariance is described. This reformulation emphasizes the importance of a geometrical factor: the slope of the separatrices of the wave flow. Its physical relevance is illustrated by two model systems: waves destabilizing open shear flows; and thermal Rossby waves in spherical shell convection with rotation. In the case of shear-flow waves, a new expression of the Reynolds–Orr amplification mechanism is obtained, and a good understanding of the form of the mean pressure and velocity fields created by weakly nonlinear waves is gained. In the case of thermal Rossby waves, results of a three-dimensional code using no-slip boundary conditions are presented in the nonlinear regime, and compared with those of a two-dimensional quasi-geostrophic model. A semi-quantitative agreement is obtained on the flow amplitudes, but discrepancies are observed concerning the nonlinear frequency shifts. With the quasi-geostrophic model we also revisit a geometrical formula proposed by Zhang to interpret the form of the zonal flow created by the waves, and explore the very low Ekman-number regime. A change in the nature of the wave bifurcation, from supercritical to subcritical, is found.

1. Introduction

In hydrodynamic stability theory and turbulence modelling, it is natural and customary to separate the velocity field into a mean flow V and a fluctuating part v. In the Navier–Stokes equation for V, the nonlinear term expressing the feedback of the fluctuating flow onto the mean flow is usually written as the divergence of the Reynolds stress tensor

$$\tau = -\langle v \otimes v \rangle, \tag{1.1}$$

where the angle brackets indicate a suitable averaging. A good understanding or modelling of τ is therefore required to explain the form of the mean flow, and other mean properties of the flow, such as the flow rate and head losses, in the case of an open system for instance. The tensor τ is also quite important for energy since in purely hydrodynamical systems its contraction with the mean strain rate tensor is the only possible source of growth of the fluctuating kinetic energy, as shown in a landmark paper by Reynolds (1895) (more recent references are, e.g. Huerre & Rossi 1998; Schmid & Henningson 2001). It is therefore of interest to develop a physical understanding of the link between the form of the fluctuating velocity field v and the

form of the Reynolds stress tensor $\boldsymbol{\tau}$, and to go beyond the tautological interpretation of $\tau_{ij} = -\langle v_i v_j \rangle$ as a correlation between v_i and v_j.

One attempt to develop such understanding was made by Busse (1983) in the case of a fluctuating field corresponding to a columnar quasi-two-dimensional wave. He noted in his §3 (see also his figure 3), a link between the variations of the 'phase function' of the wave and the relevant cross-diagonal Reynolds stress, which was revisited by Zhang (1992). The reformulation proposed by Zhang for the Reynolds stress, however, is limited to a special form of the streamfunction. In the somewhat more general case of a two-dimensional, x, y, fluctuating field, Pedlosky (1987) established (§7.3, p. 502) a link between the product $v_x v_y$ that controls the most important Reynolds stress, i.e. the cross-diagonal stress τ_{xy}, and the slope of the streamlines of $\boldsymbol{v}$. Pedlosky offered no simple formula for the average $\langle v_x v_y \rangle$, however.

The primary aim of this paper is to complement these pioneering works by proposing, in the framework of hydrodynamic stability theory, a general reformulation of the Reynolds stresses created by pure two-dimensional waves.

A first version of our Reynolds-stress reformulation was given implicitly in Plaut & Busse (2002) (§4.2; figure 5) and more explicitly in Plaut & Busse (2005) (§§7 and 8; figures 10 and 11). In both cases 'Cartesian' quasi-geostrophic (QG) models of rotating convection in a closed container were studied: a small-gap approximation was used to unfold the natural annular geometry of the systems. Here, we wish to demonstrate applications of the Reynolds-stress reformulation to a quite different family of Cartesian systems, i.e. open shear flows. In §2, we will obtain a geometric reformulation of the power injected by a basic shear flow into a wavy perturbation, which will allow an accurate analysis of the Reynolds–Orr amplification mechanism. We shall also revisit the results of Reynolds & Potter (1967) concerning the transition to Tollmien–Schlichting waves in plane channel flow, and show that a better understanding of various properties of this shear-flow instability is gained. Incidentally, the method used here to obtain the Reynolds-stress reformulation offers an interpretation of the argument of the complex wave-streamfunction, or 'phase function'; this will be illustrated by a brief study of Kelvin–Helmholtz waves.

The extension of the Reynolds-stress reformulation to the case of a 'cylindrical' axisymmetric system, i.e. in the presence of curvature effects, is also of interest. It will be given in §3, where we will focus on the thermal Rossby waves that appear as convection instabilities in a rotating spherical shell, used as a model for the liquid cores of terrestrial planets. Our approach relies on the use of a simplified two-dimensional QG convection model which has to be solved in the equatorial annulus (figure 5a). This model is similar to those developed by Aubert, Gillet & Cardin (2003), Morin & Dormy (2004, 2006), Cole (2004), Gillet & Jones (2006) and Gillet *et al.* (2007). Whereas systematic comparisons with corresponding experiments have been given in this latter paper, systematic comparisons of these QG models with realistic three-dimensional numerical models, such as Simitev & Busse (2003), have been confined to the linear regime (Aubert *et al.* 2003; Cole 2004; Gillet *et al.* 2007). In order to fill this gap, we will present new 'benchmarking' results from the three-dimensional code of Tilgner & Busse (1997) and Simitev & Busse (2003). These results represent the first complete set of data concerning weakly nonlinear waves in a spherical shell convection model with no-slip boundary conditions. (To our knowledge the only published data concerning mean flows for instance, which appear to be an important feature of nonlinear thermal Rossby waves, in a spherical shell convection model with no-slip boundary conditions are those of Aurnou & Olson (2001). The Rayleigh number used by these authors was roughly six times critical.) Thus, a systematic comparison

between the three- and two-dimensional models will be performed. This comparison, which 'validates' the two-dimensional QG model as far as the flow amplitudes are concerned, is of interest by itself in the field of geophysical fluid dynamics. It will also demonstrate the relevance of our geometrical analysis for a three-dimensional problem. Finally, a study of the QG model at very low Ekman number, where the three-dimensional codes cannot operate because of numerical difficulties, will show a transition to a subcritical regime. This result confirms a conjecture by Proctor (1994) inspired by Soward (1977), and complements Cole (2004).

2. Case of waves breaking a translational invariance

2.1. *'Cartesian' framework and model systems*

We consider a pure two-dimensional wave breaking the translational invariance, in the x-direction, of a basic flow $V_0(y) = U_0(y)e_x$ of an incompressible fluid. Because of this assumption, the velocity field of the wave can be written in term of a streamfunction,

$$v = Av_1 + \text{c.c.} \tag{2.1a}$$

with

$$v_1 = (\partial_y \psi_1)e_x - (\partial_x \psi_1)e_y, \quad \psi_1 = \Psi_1(y) \exp[i(qx - \omega t)]. \tag{2.1b}$$

In this equation, A is a (small) complex amplitude, $\Psi_1(y)$ the complex wave stream-function, q the wavenumber, ω the wave angular-frequency. Whenever the wave appears through a bifurcation, i.e. when a reduced control parameter ϵ goes through 0, a weakly nonlinear analysis can be performed. It yields a sharper model of the velocity field

$$u = V_0 + (Av_1 + \text{c.c.}) + |A|^2 V_2 + (A^2 v_2 + \text{c.c.}). \tag{2.2}$$

There, the corrections of order A^2,

$$V_2 = U_2(y)e_x, \tag{2.3}$$

$$v_2 = (\partial_y \psi_2)e_x - (\partial_x \psi_2)e_y \quad \text{with} \quad \psi_2 = \widetilde{\Psi}_2(y) \exp[2i(qx - \omega t)], \tag{2.4}$$

are calculated by a quasi-static elimination. The Reynolds stresses generated by the linear wave (2.1) feed the mean-flow correction $V_2(y)$ and the associated pressure field $P_2(x, y)$, as will be discussed in §§ 2.2 and 2.3. The amplitude A can be calculated by pushing further the weakly nonlinear analysis, to obtain at order A^3 the Landau equation

$$\tau_0 dA/dt = \epsilon(1 + ic_0)A - g(1 + ic_1)|A|^2 A, \tag{2.5}$$

with the characteristic time τ_0, the saturation coefficient g, and the linear (resp. nonlinear) frequency-shift coefficient c_0 (resp. c_1).

The basic flow could be the Poiseuille flow $U_0(y) = 1 - y^2$ or any other parallel shear flow; in such cases Ψ_1 appears as an eigenmode of the linearized vorticity equation. An example of streamlines of a total flow $V_0 + v$, neglecting the terms of order greater than A^2, is shown in figure 1. We may also consider thermohydrodynamical systems, e.g. Rayleigh–Bénard convection. In this case $V_0 = 0$, and the corresponding rolls are 'waves' in a loose sense, since the angular frequency $\omega = 0$. It is convenient to use a dimensionless formulation. For instance for Poiseuille flow, the unit of length (resp. velocity) is the half-channel width h (resp. the centreline velocity U) and the Reynolds number is $Re = Uh/\nu$ with ν the kinematic viscosity; consequently $\epsilon = Re/Re_c - 1$
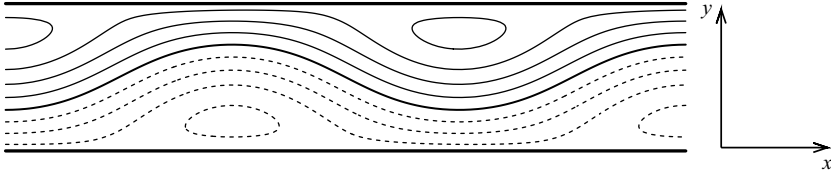
FIGURE 1. Example of a 'Cartesian' system to which our analysis applies: the critical Tollmien–Schlichting wave destabilizing plane Poiseuille flow. The streamlines of the total flow $V_0 + v$ (see (2.1) and (2.2)) are shown with the following conventions, used throughout this paper: the continuous (resp. dashed) thin lines show levels where the streamfunction is positive (resp. negative), whereas the thick lines show the levels where the streamfunction vanishes.

with $Re_c = 5772$ (Reynolds & Potter 1967). In all cases, a spectral code has been used to compute the flows.

2.2. *Reformulation of the diagonal Reynolds stresses and consequences*

The diagonal Reynolds stresses generated by the wave flow (2.1) can be written as

$$\tau_{xx} = -2E_{cx}, \quad \tau_{yy} = -2E_{cy}, \tag{2.6a}$$

with the longitudinal kinetic energy of the wave flow

$$E_{cx} = \tfrac{1}{2}\left\langle v_x^2 \right\rangle_x = |A|^2 |\Psi_1'(y)|^2, \tag{2.6b}$$

and the transverse kinetic energy of the wave flow

$$E_{cy} = \tfrac{1}{2}\left\langle v_y^2 \right\rangle_x = |A|^2 q^2 |\Psi_1(y)|^2. \tag{2.6c}$$

Hereinafter, we denote the average in directions of coordinates with angle brackets and these coordinates as indices; 'longitudinal' refers to the direction of invariance of the basic configuration, 'transverse' to the perpendicular direction. Thus, the modulus of the complex streamfunction $|\Psi_1|$ defines the transverse kinetic energy, which, for systems where no-slip boundary conditions apply and where a mid-plane mirror symmetry under $y \mapsto -y$ exists, assumes a simple form visible in figures 2(*b*) and 2(*d*).

The Reynolds stress τ_{yy} appears in the transverse component of the mean Navier–Stokes equation at order $|A|^2$,

$$0 = -|A|^2 P_2'(y) + \tau_{yy}'(y), \tag{2.7a}$$

written here for plane channel flow, with $P_2(y)$ the y-dependent part of the correction to the mean pressure field created by the waves (for the x-dependent part of the pressure field at order $|A|^2$, see §2.3). Integration of (2.7a) yields

$$P_2(y) = \tau_{yy}(y)/|A|^2 + P_{20} = -2E_{cy}/|A|^2 + P_{20}, \tag{2.7b}$$

which means that τ_{yy} drives a pressure drop in the middle of the channel, as compared with the pressure levels at the sidewalls.

2.3. *Reformulation of the cross-diagonal Reynolds stress and first consequences*

Contrary to the case of the diagonal Reynolds stresses τ_{xx} and τ_{yy}, it is not straightforward to interpret the cross-diagonal Reynolds stress τ_{xy}. By definition,

$$\tau_{xy} = -\left\langle v_x v_y \right\rangle_x = 2q|A|^2 \mathrm{Im}[\Psi_1'(y)\Psi_1^*(y)], \tag{2.8}$$

an equation which is usually plugged in a computer code to evaluate τ_{xy}, as was done for instance by Reynolds & Potter (1967) in the case of plane channel flow. However,
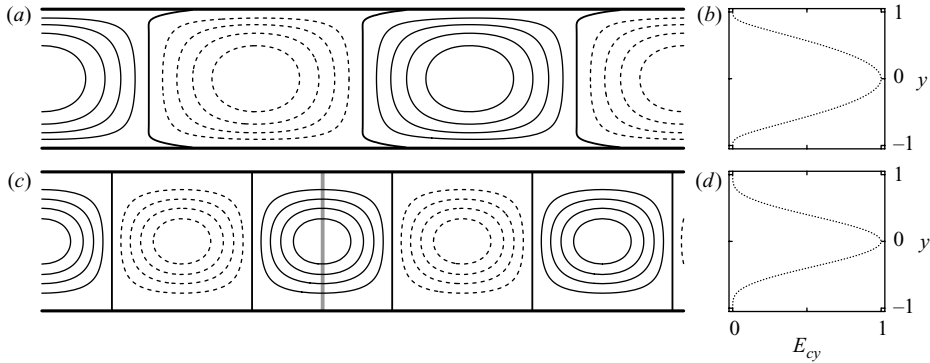
FIGURE 2. (*a*) Streamlines of the critical Tollmien–Schlichting wave flow $\boldsymbol{v}$ (see (2.1)). (*b*) Corresponding transverse kinetic energy E_{cy}. (*c,d*) Same plots for the Rayleigh–Bénard convection rolls. The grey line in (*c*) shows the mirror advocated in (2.11).

a physical reformulation of the Reynolds stress τ_{xy} is possible if we concentrate, first, on the separatrices of the wave flow (2.1). These curves are the loci of the points where the wave streamfunction vanishes,

$$\psi = A\psi_1 + \text{c.c.} = 2|A\Psi_1(y)| \cos\{qx - \omega t + \arg[\Psi_1(y)] + \arg(A)\} = 0.$$

They are therefore given by

$$x = x_s(y) = -q^{-1} \arg[\Psi_1(y)] + \lambda/4 + n\lambda/2 + ct - q^{-1} \arg(A) \qquad (2.9)$$

for $n \in \mathbb{Z}$, with $\lambda = 2\pi/q$ the wavelength, $c = \omega/q$ the wave speed. The dependence on t, which may also arise from the term $\arg(A)$, is simple, and may be neglected. Thus, the curves $x_s(y)$ (examples of which are given by the thick lines in figures 2*a* and 2*c*) give direct access to the argument of the complex streamfunction $\Psi_1(y)$. Combining (2.6), (2.8) and (2.9) gives the desired formula,

$$\tau_{xy} = -2E_{cy}x_s' = \tau_{yy}x_s', \qquad (2.10)$$

denoting with a prime the derivative with respect to the transverse coordinate y; note that the slope of the separatrices $x_s' = \tan\alpha$ with α a 'tilt angle' as shown in figure 3(*a*).

The presence of the factor $x_s' = -q^{-1}\text{d}\arg(\Psi_1)/\text{d}y$ proves, in a general case, the statement by Busse (1983) that if the phase of the wave is independent of the transverse coordinate, no Reynolds stress arises. From a more geometrical point of view, this means that, despite the existence of a kinetic energy, wave flows with straight transverse separatrices, like standard convection rolls (figure 2*c*), have $\tau_{xy} = 0$. It is equivalent to having straight separatrices that the complex streamfunction $\Psi_1(y)$ has a constant phase, i.e. that it can be chosen real, or that the wave flow (2.1) presents the 'transverse mirror' symmetry property (given in detail hereinafter for the case where A and Ψ_1 are real)

$$x \mapsto 2ct - x \quad \Longrightarrow \quad \psi \mapsto \psi, \quad v_x \mapsto v_x, \quad v_y \mapsto -v_y. \qquad (2.11)$$

On the contrary, less symmetric wave flows such as the Tollmien–Schlichting wave flow possess sloping separatrices, at least in the boundary layers near the sidewalls (figure 2*a*): they therefore generate cross-diagonal Reynolds stresses. This is because these purely hydrodynamical waves extract their energy from the basic shear flow, as
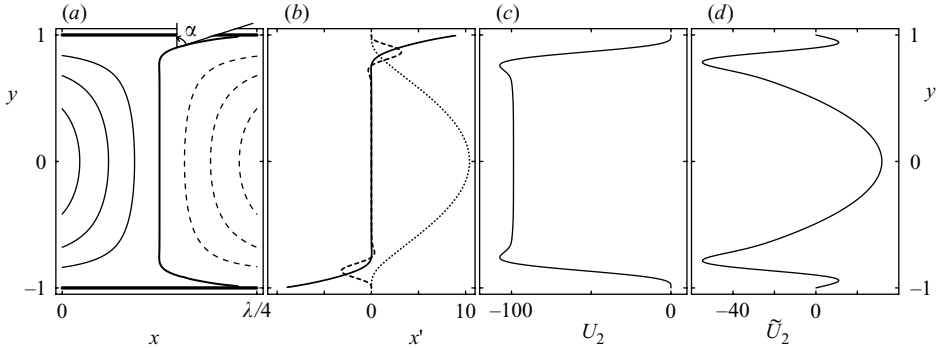
FIGURE 3. (a) Zoom on a separatrice between two cells of a Tollmien–Schlichting wave. (b) Plots illustrating (2.10) and (2.14b): the dotted line is $10E_{cy}$, the continuous line is the slope of the separatrice $x'_s = \tan\alpha$, the dashed line is the product $40E_{cy}x'_s$, indicating the profile of the opposite of the Reynolds stress τ_{xy}. (c) Mean-flow correction U_2 calculated for fixed pressure drop with (2.14b). (d) Mean-flow correction $\tilde{U}_2$ calculated for fixed flow rate with (2.16c).

shown by the Reynolds–Orr energy equation truncated at order $|A|^2$,

$$\mathrm{d}\langle E_{cx} + E_{cy}\rangle_y /\mathrm{d}t = -Re^{-1}\langle \nabla(\boldsymbol{v}) : \nabla(\boldsymbol{v})\rangle_{xy} + \langle \tau_{xy}(y)U'_0(y)\rangle_y. \tag{2.12}$$

The first term in the right-hand side, due to dissipation, is always negative. The second term can be positive if regions where

$$\tau_{xy}(y)U'_0(y) = -2E_{cy}(y)x'_s(y)U'_0(y) > 0, \quad \text{i.e.} \quad x'_s(y)U'_0(y) < 0, \tag{2.13}$$

exist and are predominant. This means, loosely speaking, that, for the wave flow to extract energy from the basic mean flow, the separatrices must slope 'against' this mean flow. In the case of plane Poiseuille flow, since $U'_0(y) > 0$ (resp. < 0) for $y < 0$ (resp. > 0), we understand why the separatrices slope 'backward' (resp. 'forward') near the inferior (resp. superior) sidewall, as shown in figures 2(a) and 3(a). Note that this analysis makes more precise the interpretation given by Pedlosky (1987) of the Reynolds–Orr amplification mechanism; for a detailed discussion see the Appendix.

Non-vanishing values of τ_{xy} do not only play a role in the mechanism of instability of hydrodynamical waves, they also modify the mean flow at nonlinear order $|A|^2$. This can be seen by considering the longitudinal component of the mean Navier–Stokes equation at this order,

$$0 = Re^{-1}|A|^2 U''_2(y) + \tau'_{xy}(y), \tag{2.14a}$$

focusing first on the case of plane channel flow with a fixed pressure drop. This equation can be integrated once, and because of the symmetry of U_2 and τ_{xy} under $y \mapsto -y$, we obtain

$$U'_2(y) = -Re\,\tau_{xy}(y)/|A|^2 = 2Re\,E_{cy}(y)x'_s(y)/|A|^2, \tag{2.14b}$$

which is illustrated in figure 3(b). Because of (2.13), we have predominantly

$$U'_2(y)U'_0(y) < 0, \tag{2.15}$$

i.e. the modification of the mean flow due to the waves acts against this mean flow. This is confirmed by a further integration of (2.14b), which yields the mean-flow profile shown in figure 3(c). This means physically that, when the transition to Tollmien–Schlichting waves develops, the flow rate is reduced in channel flow with a fixed pressure drop. Alternatively, fixed flow rate conditions can be imposed, i.e.

Model	g	$\mathrm{Re}(G_{12})$	$\mathrm{Re}(G_{21})$	$\mathrm{Re}(g_{12})$	$\mathrm{Re}(g_{21})$
Fixed pressure drop	-3059	-5475	$+1410$	$+5312$	-4306
Fixed flow rate	-3189	-5320	$+1125$	$+5312$	-4306

TABLE 1. Values of the Landau constant g at the bifurcation to Tollmien–Schlichting waves in plane Poiseuille flow, and of the different terms that contribute to g (see (2.17))

a correction $\widetilde{P}_2' x$ to the pressure field can be introduced at order $|A|^2$ such that the modified mean-flow correction $\widetilde{U}_2$ satisfies

$$\langle \widetilde{U}_2(y) \rangle = 0. \tag{2.16a}$$

Thus, the longitudinal component of the mean Navier–Stokes equation at order $|A|^2$ now reads

$$0 = -|A|^2 \widetilde{P}_2' + Re^{-1}|A|^2 \widetilde{U}_2''(y) + \tau_{xy}'(y), \tag{2.16b}$$

which, by comparison with (2.14a), gives

$$\widetilde{U}_2(y) = U_2(y) + \tfrac{1}{2} Re\, \widetilde{P}_2'(y^2 - 1) \quad \text{where} \quad \widetilde{P}_2' = \tfrac{3}{2} Re^{-1} \langle U_2(y) \rangle_y < 0. \tag{2.16c}$$

The mean-flow correction $\widetilde{U}_2$ is shown in figure 3(d), which corresponds to figure 3(c) of Reynolds & Potter (1967). The fact that the mean pressure gradient $\widetilde{P}_2'$ given by (2.16c) is negative indicates another generic feature of transitions (here to Tollmien–Schlichting waves, but we may generalize) in shear flows: in a system with a fixed flow rate, such transitions imply an increase of the head loss.

2.4. *Further consequence: subcritical nature of the Tollmien–Schlichting bifurcation*

It is a known numerical fact that, for the Tollmien–Schlichting critical wave destabilizing plane Poiseuille flow, the Landau constant g in (2.5) is negative. This happens both for fixed pressure drop (Herbert 1980) and fixed flow-rate conditions (Reynolds & Potter 1967; Fujimura 1987). In order to show that the feedback of the mean-flow correction V_2 onto the wave plays an important role in this phenomenon, we present a detailed study of the terms that control the value of g. Introducing the adjoint critical streamfunction $\psi_a = \Psi_a(y)\exp[\mathrm{i}(qx - \omega t)]$ solution of equation (3.6a) of Reynolds & Potter (1967), the notations $\zeta(\boldsymbol{u}) = \partial_x(u_y) - \partial_y(u_x)$ to designate the vorticity of a field $\boldsymbol{u}$, the asterisk to designate the complex conjugates, and the normalization conditions $\Psi_1(0) = 1$, $\langle \zeta(\boldsymbol{v}_1)\psi_a^* \rangle_{xy} = \tau_0 = 103.0$, we have

$$g(1 + \mathrm{i}c_1) = G_{12} + G_{21} + g_{12} + g_{21} \tag{2.17a}$$

with

$$G_{12} = \langle \boldsymbol{v}_1 \cdot \nabla \zeta(V_2)\,\psi_a^* \rangle_{xy}, \quad g_{12} = \langle \boldsymbol{v}_1^* \cdot \nabla \zeta(\boldsymbol{v}_2)\,\psi_a^* \rangle_{xy}, \\ G_{21} = \langle V_2 \cdot \nabla \zeta(\boldsymbol{v}_1)\,\psi_a^* \rangle_{xy}, \quad g_{21} = \langle \boldsymbol{v}_2 \cdot \nabla \zeta(\boldsymbol{v}_1^*)\,\psi_a^* \rangle_{xy}. \tag{2.17b}$$

The values of table 1 agree with published precise computations, $g/\tau_0 = -a_1$ (Herbert) $= -29.69$ for fixed pressure drop, $g/\tau_0 = -\lambda_{1r}$ (Fujimura) $= -30.96$ for fixed flow rate. Table 1 shows that the most negative term contributing to g is $\mathrm{Re}(G_{12})$.

2.5. *Another canonical example: inviscid Kelvin–Helmholtz instability*

The inviscid instability of the hyperbolic-tangent velocity profile

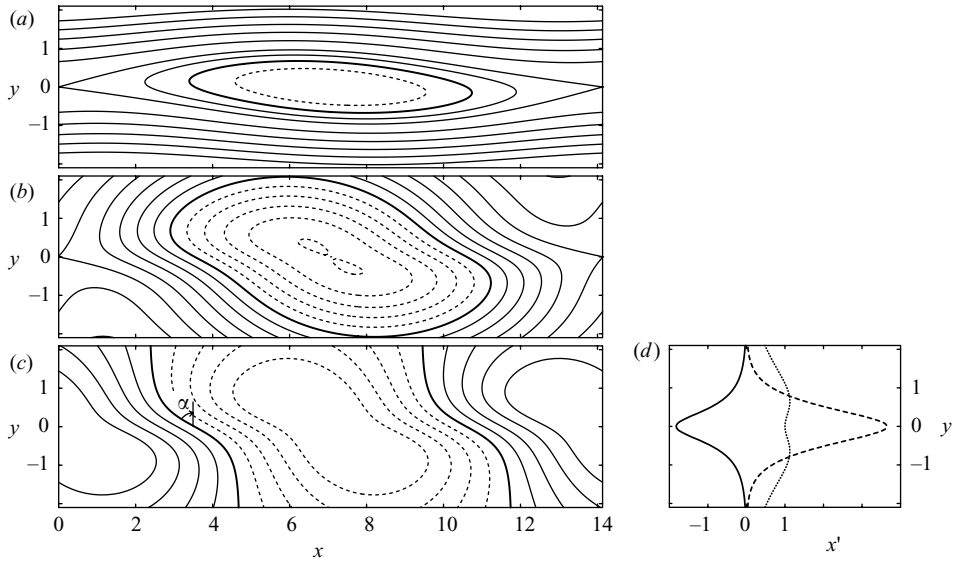$$\boldsymbol{V}_0 = U_0(y)\boldsymbol{e}_x = \tfrac{1}{2} \tanh y\,\boldsymbol{e}_x, \tag{2.18}$$

FIGURE 4. Most-amplified Kelvin–Helmholtz wave destabilizing the shear-layer profile (2.18).
(*a*) Streamlines of the total flow $V_0 + v$, with a wave-amplitude $A = 0.1$. (*b*) The same, but
with a larger wave amplitude $A = 1$. (*c*) Streamlines of the wave flow v_1 alone, i.e. '$A = \infty$'.
(*d*) Kinetic energy E_{cy} (dotted line), slope x_s' (continuous line) and Reynolds stress τ_{xy} (dashed
line).

has been studied in a seminal paper by Michalke (1964), who showed that, in agree-
ment with the Fjørtoft's criterion, this shear flow is unstable vs. Kelvin–Helmholtz
waves. Michalke (1964) shows in his figures 4 and 5 the real and imaginary parts of
the complex wave-streamfunction $\Psi_1(y)$; from these graphs we can deduce that, for
the most-amplified mode (of wavenumber $q = 0.4446$),

$$\arg[\Psi_1(y)] = \arctan\{\mathrm{Im}[\Psi_1(y)]/\mathrm{Re}[\Psi_1(y)]\}$$

is an increasing phase function of y for small $|y|$. This means, according to our (2.9),
that the separatrices $x_s(y)$ of the corresponding wave slope backward in the shear
layer, a result that we could also deduce from the criterion (2.13). By use of the
result of the Appendix, we expect that, on average, the streamlines of the total flow
$V_0 + v$ slope backward. Yet, in the corresponding figure 7 (top) of Michalke
(1964), on average the streamlines slope forward. By reproducing the computations of Michalke
(1964), we have found that the correct plot of the total-flow streamlines is as shown in
our figure 4(*a*). (Otherwise we agree completely with Michalke. A figure similar to our
figure 4(*a*) has been published by Corcos & Sherman (1984), who, however, studied
a slightly different basic flow.) We have complemented it with figures 4(*b*) and (*c*) to
illustrate our reasoning, and show explicitly the form of the separatrices $x_s(y)$ in this
case. In addition, figure 4(*d*) displays a Reynolds-stress profile that can be understood
from (2.10), and that is quite close to that obtained in mixing-layer experiments, as
shown, for instance, in the first plot of figure 20 of Ho & Huerre (1984).

3. Case of waves breaking a rotational invariance

In contrast to §2, we start here by exhibiting a three-dimensional physical problem
where a wave breaks the rotational invariance around the axis Oz of a basic flow state
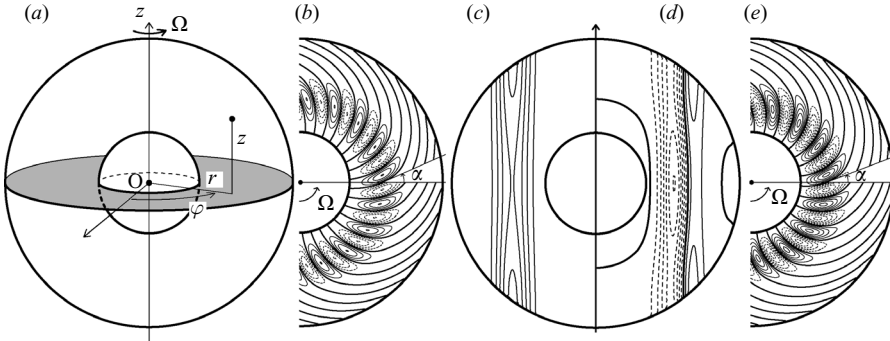
FIGURE 5. (*a*) Example of a 'cylindrical' system to which our analysis applies: the convection of a fluid contained between an inner sphere of radius r_i and an outer sphere of radius r_o. The solid rotation of these spheres around the axis Oz imposes, because of the Proudman–Taylor constraint, the cylindrical character of the flow. Thus, the QG model considers z-averaged fields defined in the (grey) equatorial annulus. (*b*) In this annulus, for $E = 2 \times 10^{-5}$, $\epsilon = Ra/Ra_c - 1 = 0.01$, radial velocity v_r of the saturated critical wave computed with the three-dimensional code. (*c*) In a meridional cut, maximal values of v_r with respect to φ, i.e. $2|U_1|$ with U_1 the radial component of $\boldsymbol{V}_1$ in (3.1*a*). (*d*) In a meridional cut, azimuthal mean flow V generated by this wave. (*e*) In the equatorial annulus, radial velocity v_r of the saturated critical wave computed with the two-dimensional QG model for the same parameters. Contour steps are 1 for v_r in (*b*), (*c*) and (*e*), 0.025 for V in (*d*). The sectors in (*b*) and (*e*) show tilt angles α (3.18) at the critical radii.

$\boldsymbol{V}_0(r, z)$, and return only afterwards to the general two-dimensional framework for the study of Reynolds stresses. The triplet (r, φ, z) designates cylindrical coordinates.

3.1. *Original model system: convection in a rotating spherical shell*

Convection in a rotating spherical shell (figure 5*a*) is used as a model for convection in planets or stars (Busse 2002). Here, we consider standard Boussinesq models as defined for instance in Simitev & Busse (2003): the fluid has a constant coefficient of thermal expansion a, kinematic (thermal) diffusivity ν (κ). For simplicity, we focus on a single heating mode, for which asymptotic linear theories are available both for the three-dimensional model introduced here and for the reduced model introduced in the next subsection. We assume that internal heat sources exist in the fluid, which create a basic temperature gradient $\nabla T_b = -b\boldsymbol{x}$ with $\boldsymbol{x}$ the position vector with respect to the centre of the sphere. In the representative case of a Prandtl number $P = \nu/\kappa = 1$ and of a fixed radius ratio $\eta = r_i/r_o = 0.35$, the model depends on two control parameters: the Ekman number $E = \nu/(\Omega d^2)$ with Ω the angular velocity of the spheres, $d = r_o - r_i$ the shell size, and the Rayleigh number $Ra = abcd^6/(\nu\kappa)$, with c the coefficient defining the gravity field $-c\boldsymbol{x}$ (Ra is denoted by R_i in Simitev & Busse 2003). Note that the values of the Ekman number are expected to be small in planets. When Ra exceeds a critical value that increases with decreasing E, the basic conductive state, which corresponds to a velocity field $\boldsymbol{V}_0 = \boldsymbol{0}$ in the rotating frame, loses its stability against a progradely travelling thermal Rossby wave of velocity field

$$\boldsymbol{u} = \boldsymbol{v} = \boldsymbol{V}_1(r, z) \exp[\mathrm{i}(m\varphi - \omega t)] + \text{c.c.} \tag{3.1a}$$

and temperature perturbation field

$$\theta = T - T_b = \Theta_1(r, z) \exp[\mathrm{i}(m\varphi - \omega t)] + \text{c.c.} \tag{3.1b}$$

where $m \in \mathbb{N}^*$ is the wavenumber, $\omega \in \mathbb{R}^{+*}$ the wave angular frequency. Such a wave (figure 5*b*) does break the rotational symmetry of the basic flow. For a theoretical study of this linear instability, and a global asymptotic analysis of its form as $E \to 0$, where one observes that $V_1(r, z)$, $\Theta_1(r, z)$ localize around a critical radius r_c (figure 5*c*), see Jones, Soward & Mussa (2000) and Dormy *et al.* (2004). Through nonlinear effects, a wave of the form (3.1) generates naturally harmonic waves of wavenumbers $\pm 2m, \pm 3m, \ldots$, but also a mean or 'zonal' flow of zero wavenumber (figure 5*d*). These waves have attracted attention because, in the presence of magnetohydrodynamical effects, they may be subject to a secondary dynamo instability leading to a self-sustained magnetic field showing similarities with certain planetary fields (see e.g. Busse 2002; Simitev & Busse 2005); in particular, their zonal flow plays an important role in the dynamo mechanisms (Kageyama & Sato 1997). Note also that the bifurcation to the thermal Rossby waves is generally supercritical (Tilgner & Busse 1997), but that the possibility that it becomes subcritical for $E \ll 1$ has been suspected from the results of Soward (1977), see Proctor (1994). Indeed, Soward (1977) constructed nonlinear convection solutions at a Rayleigh number asymptotically close to the critical value predicted by the local asymptotic theory (of Busse 1970), which he also showed to be significantly smaller than the correct critical value (given precisely later, in the limit of focus $E \to 0$, by the global theory of Jones *et al.* 2000). Whereas many numerical studies of nonlinear convection have been realized with models assuming stress-free boundary conditions at the inner and outer spheres (e.g. Tilgner & Busse 1997; Christensen 2002; Simitev & Busse 2003), we prefer to focus here on models with no-slip boundary conditions, which are probably more realistic as far as cores of terrestrial planets are concerned. Another advantage of these models is that the mean flow is fully determined by the Navier–Stokes equation, whereas in the stress-free models, for pure waves the Navier–Stokes equation defines the mean flow up to a solid-body rotation component only: another model equation is required (e.g. angular momentum conservation) to determine this component, i.e. the frame of reference. A drawback of the no-slip models, however, is that their resolution is computationally more demanding because very thin Ekman layers have to be computed. Therefore they have scarcely been studied in the nonlinear regime. We should mention Aurnou & Olson (2001) and Christensen *et al.* (2001) case 0, but these authors considered another heating mode without heat sources in the fluid. The lack of data concerning thermal Rossby waves near onset in internal heating models with no-slip boundary conditions has motivated us to use the code of Simitev & Busse (2003) to obtain new quantitative results.

3.2. *Reduced quasi-geostrophic model – general 'cylindrical' framework*

The zonal flows obtained numerically, such as the one in figure 5(*d*), are difficult to explain mechanistically, because of the intrinsic complexity of the three-dimensional model. Fortunately, simpler two-dimensional models can be developed because, for $E \ll 1$, the Proudman–Taylor constraint imposes a 'columnar form' on the wave flows. These QG models rely on an axial averaging, along z, of the fields and equations, see e.g. Busse (1970), Busse & Hood (1982), Busse & Or (1986) and the papers cited §1. We present here a QG model different from those studied in Plaut & Busse (2002); Plaut & Busse (2005) because we relax the small-gap approximation and include Ekman pumping effects in a more systematic way.

For a detailed presentation of the three-dimensional model, see Simitev & Busse (2003), and for details on the calculation of the Ekman pumping terms, see Aubert *et al.* (2003), Schaeffer & Cardin (2005), Gillet & Jones (2006). Below, we use d as

unit of length, d^2/ν as unit of time and $\nu^2/(acd^4)$ as unit of temperature. Assuming that essentially the flow takes place outside of the tangent cylinder, i.e. for $r \in [r_i, r_o]$, we consider in the QG model that $u_r, u_\varphi, \partial_z u_z$ and θ do not depend on z in the bulk of the fluid, outside of the thin boundary layers (Gillet & Jones 2006). The expression for the Ekman pumping flow through the layer at $z = H = \sqrt{r_o^2 - r^2}$ gives the boundary condition for the bulk flow

$$r u_r + H u_z(z = H) = \tfrac{1}{2} E^{1/2} r_o^{1/2} H^{1/2} F_E(\boldsymbol{u}) \tag{3.2a}$$

with

$$F_E(\boldsymbol{u}) = -\zeta(\boldsymbol{u}) + r H^{-2}(\partial_\varphi u_r) - \tfrac{1}{2} r H^{-2} u_\varphi - \tfrac{5}{2} r_o r H^{-3} u_r, \tag{3.2b}$$

$$\zeta(\boldsymbol{u}) = r^{-1}[\partial_r(r u_\varphi) - \partial_\varphi u_r] \text{ the axial vorticity.} \tag{3.2c}$$

Therefore, in the bulk of the fluid,

$$u_z = -r z H^{-2} u_r + \tfrac{1}{2} z r_o^{1/2} H^{-3/2} E^{1/2} F_E(\boldsymbol{u}). \tag{3.3}$$

Taking the axial average of the axial component of the curl of the Navier–Stokes equation (1a) of Simitev & Busse (2003), using (3.3) to express the Coriolis term, and assuming the simplest approximation for the nonlinear terms, we obtain the QG vorticity equation

$$\partial_t \zeta(\boldsymbol{u}) + \boldsymbol{u} \cdot \nabla \zeta(\boldsymbol{u}) + 2 E^{-1} H^{-2} r u_r = \Delta \zeta(\boldsymbol{u}) - \partial_\varphi \theta + f_E F_E(\boldsymbol{u}), \tag{3.4a}$$

with $f_E = E^{-1/2} r_o^{1/2} H^{-3/2}$ the first Ekman pumping coefficient. Similarly, the axial average of the heat equation (1c) of Simitev & Busse (2003) (with the Prandtl number $P = 1$),

$$\partial_t \theta + \boldsymbol{u} \cdot \nabla \theta = \Delta \theta + Ra(r u_r + z u_z),$$

yields, because of (3.3),

$$\partial_t \theta + \boldsymbol{u} \cdot \nabla \theta = \Delta \theta + \tfrac{2}{3} Ra r u_r + \tfrac{1}{6} Ra g_E F_E(\boldsymbol{u}), \tag{3.4b}$$

with $g_E = E^{1/2} r_o^{1/2} H^{1/2}$ the second Ekman pumping coefficient. In order to avoid the creation of an unphysical mean pressure gradient in the annulus (see e.g. Plaut & Busse 2002; Plaut 2003), (3.4a) has to be supplemented by the mean component of the azimuthal Navier–Stokes equation,

$$\partial_t V = \Delta V - r^{-2} V - f_E V + \partial_r \tau_{r\varphi} + 2 r^{-1} \tau_{r\varphi}, \tag{3.5}$$

where $V = \langle u_\varphi \rangle_\varphi$. In (3.5), we also take into account Ekman pumping effects, and the Reynolds stress is $\tau_{r\varphi} = -\langle u_r u_\varphi \rangle_\varphi$. In accordance with the assumptions made for the three-dimensional model, we consider no-slip isothermal boundaries,

$$u_r = u_\varphi = \theta = 0 \quad \text{at} \quad r = r_i, r_o. \tag{3.6}$$

Cole (2004) studied a similar model, but with stress-free boundary conditions, and hence no Ekman pumping terms ($f_E = g_E = 0$). Morin & Dormy (2004) used no-slip boundary conditions, but neglected all Ekman pumping terms ($f_E = g_E = 0$), whereas Morin & Dormy (2006) studied the influence of the Ekman pumping effects on the mean flow (i.e. they considered that $f_E \neq 0$ in (3.5) only; note that their Ekman pumping coefficient is too small by a factor $\sqrt{2}$). Furthermore, the heat equations of the QG models of both Cole and Morin & Dormy take into account only a convection term of the form $Ra r u_r$ but omit effects of convection in the z-direction, which generate, because of (3.3), the terms $-(1/3)Ra r u_r + (1/6)Ra g_E F_E(\boldsymbol{u})$ in (3.4b).

A linear stability analysis of the conductive solution $\boldsymbol{u} = \boldsymbol{0}$ and $\theta = 0$ of (3.4) and (3.5) can be performed with normal modes that assume the form of pure waves,

$$\boldsymbol{u} = \boldsymbol{v} = A\boldsymbol{v}_1 + \text{c.c.} \tag{3.7a}$$

where

$$\boldsymbol{v}_1 = r^{-1}(\partial_\varphi \psi_1)\boldsymbol{e}_r - (\partial_r \psi_1)\boldsymbol{e}_\varphi, \quad \psi_1 = \Psi_1(r)\exp[\mathrm{i}(m\varphi - \omega t)], \tag{3.7b}$$

and

$$\theta = A\theta_1 + \text{c.c.} \quad \text{where} \quad \theta_1 = \Theta_1(r)\exp[\mathrm{i}(m\varphi - \omega t)]. \tag{3.8}$$

Before discussing the results of this analysis, we present the general form of the weakly nonlinear waves. Their velocity field is given by

$$\boldsymbol{u} = (A\boldsymbol{v}_1 + \text{c.c.}) + |A|^2\boldsymbol{V}_2 + (A^2\boldsymbol{v}_2 + \text{c.c.}) \tag{3.9}$$

where

$$\boldsymbol{V}_2(r) = V_2(r)\boldsymbol{e}_\varphi \tag{3.10}$$

is the mean or 'zonal' flow, calculated by solving a quasi-static version of (3.5) at order $|A|^2$, and where

$$\boldsymbol{v}_2 = r^{-1}(\partial_\varphi \psi_2)\boldsymbol{e}_r - (\partial_r \psi_2)\boldsymbol{e}_\varphi \quad \text{with} \quad \psi_2 = \widetilde{\Psi}_2(r)\exp[2\mathrm{i}(m\varphi - \omega t)] \tag{3.11}$$

is the harmonic flow, calculated by solving a quasi-static version of (3.4) at order A^2, identifying the terms proportional to $A^2\exp[2\mathrm{i}(m\varphi - \omega t)]$. Accordingly, the temperature deviation of weakly nonlinear waves is

$$\theta = (A\theta_1 + \text{c.c.}) + |A|^2\Theta_2 + (A^2\theta_2 + \text{c.c.}) \tag{3.12a}$$

where

$$\Theta_2 = \Theta_2(r), \quad \theta_2 = \widetilde{\Theta}_2(r)\exp[2\mathrm{i}(m\varphi - \omega t)]. \tag{3.12b}$$

At order A^3, a computation of the nonlinear terms of wavenumber m in (3.4) yields, after projection onto the adjoint critical mode, the nonlinear part of the Landau equation for the wave-amplitude (2.5), where now $\epsilon = Ra/Ra_c - 1$.

3.3. *Linear spiralling waves in rotating convection – geometry and 'tilt angle'*

The resolution of the linearized version of (3.4), accomplished numerically with a spectral method, yields the critical parameters Ra_c, m_c, ω_c and the critical mode at the bifurcation from the basic conduction state to thermal Rossby waves. A comparison with the three-dimensional results is shown in table 2, which also recalls the predictions of the global asymptotic theories available for the three-dimensional (Jones *et al.* 2000) and two-dimensional QG (Cole 2004) models in the limit of vanishing Ekman numbers; the values of the Rayleigh number given by the later theory have been divided by 2/3 (compare our equation (3.4b) with the equation (2.35) of Cole 2004). A semi-quantitative agreement is obtained between the three-dimensional and QG models if $E = 2 \times 10^{-5}$, with critical quantities that differ by less than 22%. Because of a lack of computing power, no three-dimensional data are available for $E < 2 \times 10^{-5}$, but the asymptotic regime is approached at $E = 2 \times 10^{-5}$ with critical parameters (Ra_c, m_c, ω_c) that differ by less than $(6, 4, 31)\%$ from the values predicted by Jones *et al.* (2000). On the contrary, QG results are available down to $E = 2 \times 10^{-7}$, and it can be noted that an asymptotic regime is attained if $E \leqslant 2 \times 10^{-5}$, with critical parameters (Ra_c, m_c, ω_c) that differ by less than $(7, 4, 17)\%$ from the values predicted by Cole (2004).

$E/2$	$E^{4/3}Ra_c^{3D}$	$E^{4/3}Ra_c^{2D}$	Ra_c^{2D}/Ra_c^{3D}	$E^{1/3}m_c^{3D}$	$E^{1/3}m_c^{2D}$	m_c^{2D}/m_c^{3D}
10^{-3}	3.981	3.386	0.85	0.5040	0.5040	1.00
10^{-4}	2.860	2.328	0.81	0.5263	0.4678	0.89
10^{-5}	2.621	2.060	0.79	0.4886	0.4343	0.89
10^{-6}		1.987			0.4158	
10^{-7}		1.955			0.4269	
$10^{-\infty}$	2.468	1.920	0.78	0.5086	0.4328	0.85

$E/2$	$E^{2/3}\omega_c^{3D}$	$E^{2/3}\omega_c^{2D}$	$\omega_c^{2D}/\omega_c^{3D}$
10^{-3}	0.2317	0.3814	1.65
10^{-4}	0.3688	0.4854	1.32
10^{-5}	0.4305	0.5233	1.22
10^{-6}		0.5468	
10^{-7}		0.5778	
$10^{-\infty}$	0.5616	0.6301	1.12

TABLE 2. Rescaled linear critical properties of the three-dimensional (3D) and QG two-dimensional (2D) models. The scaling laws and the results for $E = 10^{-\infty}$ correspond to the asymptotic predictions of Jones *et al.* (2000) and Cole (2004) valid in the limit $E \to 0$.

The form of the two-dimensional waves itself is close to the form of the three-dimensional waves, as is shown by the comparison between figures 5(b) and (e). On the basis of similar three-dimensional results (but with stress-free boundary conditions), and following a suggestion by Busse & Carrigan (1983), Zhang (1992) named quite appropriately such waves 'spiralling' waves. More precisely, he proposed in his introduction a simple model for the velocity field of such waves, in the spirit of the QG approximation. Applying an axial average to the three-dimensional velocity field of a pure thermal Rossby wave, one can in fact prove, by use of the solenoidal character of the field, that there exists a streamfunction ψ such that

$$\langle \boldsymbol{v} \rangle_z = r^{-1}(\partial_\varphi \psi)\boldsymbol{e}_r - (\partial_r \psi)\boldsymbol{e}_\varphi. \tag{3.13}$$

Thus, assuming that $\boldsymbol{v} \simeq \langle \boldsymbol{v} \rangle_z$, we recover the first equation of Zhang (1992), which appears to be quite relevant. On the contrary, the form of streamfunction that he proposes in his second equation is rather restrictive, whereas it is surely general to use (3.7),

$$\psi = 2|A\Psi_1(r)| \cos\{m[\varphi - \Phi(r)] - \omega t + \arg(A)\} \tag{3.14}$$

where

$$\Phi(r) = -m^{-1} \arg[\Psi_1(r)] \tag{3.15}$$

is the function generalizing Zhang's 'phase function'. This function controls both the form of the separatrices $\psi = 0$, given by

$$\varphi = \varphi_s(r) = \Phi(r) + \Lambda/4 + n\Lambda/2 + Ct - m^{-1}\arg(A), \tag{3.16}$$

with $n \in \mathbb{Z}$, $\Lambda = 2\pi/m$ the angular wavelength, $C = \omega/m$ the angular wave-speed, and the form of the isolines $v_r = 0$, given by

$$\varphi = \Phi(r) + n\Lambda/2 + Ct - m^{-1}\arg(A) = \varphi_s(r) - \Lambda/4, \tag{3.17}$$

at least within the framework of the model (3.13), i.e. assuming $v_r \simeq \langle v_r \rangle_z = r^{-1}(\partial_\varphi \psi)$ in the three-dimensional case. Clearly, spiralling waves are such that the phase function (3.15) varies significantly when r increases from r_i to r_o, i.e. such that the 'inclination'

$E/2$	r_c^{3D}/r_o	r_c^{2D}/r_o	r_c^{2D}/r_c^{3D}	α^{3D} (deg.)	α^{2D} (deg.)	α^{2D}/α^{3D}
10^{-3}	0.577	0.609	1.06	17.2	11.7	0.68
10^{-4}	0.601	0.563	0.94	19.5	15.5	0.79
10^{-5}	0.578	0.531	0.92	23.0	20.8	0.91
10^{-6}		0.521			26.8	
10^{-7}		0.532			30.9	
$10^{-\infty}$	0.592	0.554	0.94	34.2	38.3	1.12

TABLE 3. Comparison between the critical radii and the corresponding tilt angles (3.18) at onset predicted by the three-dimensional and QG two-dimensional models. The results for $E = 10^{-\infty}$ correspond to the asymptotic predictions of Jones *et al.* (2000) and Cole (2004).

or 'tilt' angle,

$$\alpha = \arctan r\varphi_s'(r) = \arctan r\Phi'(r), \tag{3.18}$$

is of order unity. Tilt angles at the 'critical radius' r_c where v_r is maximum (in the three-dimensional case these quantities have been measured in the equatorial plane) are shown in figures 5(*b*) and (*d*). Table 3 confirms the impression produced by these figures, i.e. that the tilt angles of both models are close. Note that Jones *et al.* (2000) and Cole (2004) gave asymptotic predictions for the critical radius, the phase function and the tilt angle (see e.g. Jones *et al.* 2000, pp. 171 and 178). A conclusion that can be drawn from tables 2 and 3 is that the QG model yields a semi-quantitatively valid description, with discrepancies smaller than 21%, for all properties of the linear waves, except for their frequency, as soon as $E \lesssim 2 \times 10^{-4}$.

There exists no general weakly nonlinear theory either for the three-dimensional or for the two-dimensional QG models, even at finite values of the Ekman number. Because nonlinear effects are typically quite sensitive to slight differences in models, we could fear that, in the nonlinear regime, the semi-quantitative agreement noted in the linear regime could be totally lost. We will now see that this is not the case.

3.4. *A first nonlinear effect due to Reynolds-stress: mean-flow generation*

The fact that the mean flow at order A^2 is generated by the Reynolds-stress term in (3.5) motivates the reformulation of the Reynolds-stress tensor in a general 'cylindrical' system. This reformulation will be presented in §3.4.1, and its consequence for rotating convection in §3.4.2.

3.4.1. *Reformulation of the Reynolds-stress tensor*

The diagonal Reynolds stresses generated by a pure wave of the form (3.7) are

$$\tau_{rr} = -2E_{cr}, \quad \tau_{\varphi\varphi} = -2E_{c\varphi}, \tag{3.19a}$$

where the transverse kinetic energy of the wave flow

$$E_{cr} = \tfrac{1}{2}\langle v_r^2 \rangle_\varphi = |A|^2 m^2 r^{-2}|\Psi(r)|^2 \tag{3.19b}$$

and the longitudinal kinetic energy of the wave flow

$$E_{c\varphi} = \tfrac{1}{2}\langle v_\varphi^2 \rangle_\varphi = |A|^2 |\Psi'(r)|^2. \tag{3.19c}$$

As in §2.2, we use 'transverse' and 'longitudinal' to refer the orientation with respect to the direction e_φ of invariance of the basic state.

Thus the modulus of the streamfunction is related to the transverse kinetic energy, whereas, according to (3.16), its phase is related to the separatrices. This allows us to
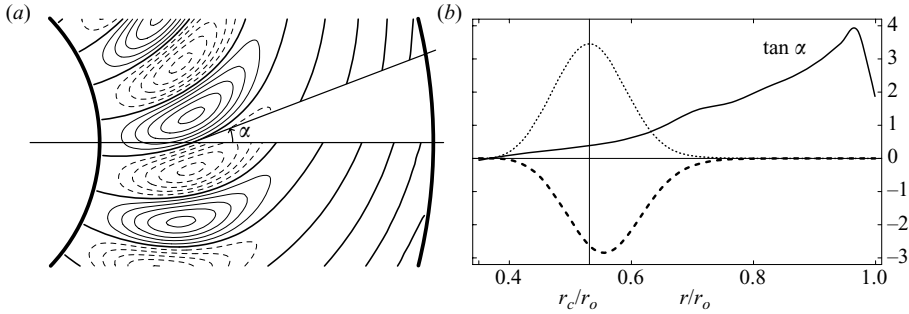
FIGURE 6. For $E = 2 \times 10^{-5}$, $\epsilon = 0.01$, with the QG model, i.e. for the wave already displayed in figure 5(*e*). (*a*) Zoom on the contours of v_r showing the tilt angle at the critical radius r_c. (*b*) The dotted line shows the factor $E_{cr}/2$, the thin line the slope $\tan\alpha$, the dashed line illustrates (3.20) by showing the product $-E_{cr}\tan\alpha$, i.e. half the Reynolds stress $\tau_{r\varphi}$.

obtain the reformulation of the cross-diagonal Reynolds-stress,

$$\tau_{r\varphi} = -\langle v_r v_\varphi \rangle_\varphi = -2E_{cr}\tan\alpha = \tau_{rr}\tan\alpha \qquad (3.20)$$

where $\alpha = \alpha(r) = \arctan r\Phi'(r)$ is the tilt angle (3.18). There is a close similarity between (3.20) and the formula (2.10) obtained in the Cartesian case. Note also that equation (1) of Zhang (1992) contains, on its right-hand side, a similar reformulation.

An illustration of (3.20) is given in figure 6, which shows that, for the spiralling Rossby wave studied, the slope $\tan\alpha$ assumes values of order 1 when $r > r_c$. On the other hand, the transverse energy E_{cr} is large only around $r \simeq r_c$. Hence a negative Reynolds stress $\tau_{r\varphi}$ of the shape shown in figure 6(*b*) is generated near $r = r_c$.

3.4.2. *Consequence in rotating convection: mean-flow generation*

At order A^2, the mean equation (3.5),

$$|A|^2[f_E V_2 - r^{-1}\partial_r(r\partial_r V_2) + r^{-2}V_2] = \partial_r\tau_{r\varphi} + 2r^{-1}\tau_{r\varphi}, \qquad (3.21)$$

shows that the Reynolds-stress $\tau_{r\varphi}$ (3.20) generates a zonal flow $V_2(r)$ in the azimuthal direction. The source terms on the right-hand side of (3.21) are dominated by the contribution of $\partial_r\tau_{r\varphi}$, as shown by the comparison of figures 6(*b*) and 7(*a*). Once these terms are calculated, (3.21) can be solved numerically, which yields the thin curve in figure 7(*b*). A crude approximation to this curve is obtained by neglecting the viscous terms in (3.21), i.e. by equilibrating the Ekman pumping term with the nonlinear term, which gives

$$|A|^2 V_2 \simeq f_E^{-1}(\partial_r\tau_{r\varphi} + 2r^{-1}\tau_{r\varphi}) \simeq f_E^{-1}\partial_r\tau_{r\varphi}. \qquad (3.22)$$

Thus, because the Reynolds stress $\tau_{r\varphi}$ decreases towards the inner part of the annulus and increases towards the outer part, we expects a retrograde (resp. prograde) zonal flow in the interior (resp. exterior). Figure 7(*b*) shows that this is qualitatively correct; a mean flow of a similar form has been obtained with a simpler, Cartesian QG model by Busse & Hood (1982), and with cylindrical QG models by Aubert *et al.* (2003), Gillet & Jones (2006), Morin & Dormy (2006). The fact that the formula (3.22) fails to describe the zonal flow amplitude quantitatively, since here for instance it would yield $\min(|A|^2 V_2) = -0.265$ instead of $\min(|A|^2 V_2) = -0.150$, underlines the importance of both dissipation mechanisms, bulk viscosity and Ekman pumping, as noticed by Gillet & Jones and Morin & Dormy.
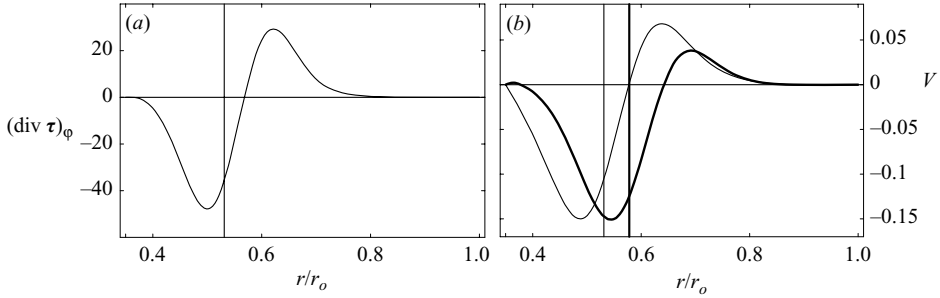
FIGURE 7. For the conditions of figure 6, with the two-dimensional (thin lines) or three-dimensional (thick line) models. (a) Azimuthal component of the divergence of the Reynolds-stress tensor, the right-hand side of (3.21). (b) Zonal flow profiles in the equatorial annulus. The vertical lines show r_c^{2D}/r_o and r_c^{3D}/r_o.

As compared to the three-dimensional mean flow (the thick curve in figure 7b), the QG mean flow attains its minimum at a smaller value of r. This is in line with the inequality $r_c^{2D} < r_c^{3D}$ (table 3). The fact that the maximum of the QG mean flow is larger than the maximum of the three-dimensional mean flow in the equatorial plane can be understood by recalling that the QG model is constructed to best describe the axially averaged flows, and by noting that figure 5(c) shows that the three-dimensional mean flow is larger out of the equatorial plane around $r = 0.65 r_o$. A remarkable result of figure 7(b) is the quantitative agreement between the minimum values of the two- and three-dimensional mean flows, which shows that the QG model correctly describes the saturation of the waves. This will now be discussed in more details.

3.5. Further nonlinear effects in rotating convection: saturation and frequency shift

The levels of v_r in figures 5(e) and 6(a), the values of E_{cr}, $\tau_{r\varphi}$ and V in figures 6(b) and 7 have been obtained after a systematic computation of the Landau equation (2.5) for the amplitude of the critical wave solution of the QG model. Starting with a critical mode normalized according to

$$\max_r [|\Psi_1(r)|/r] = 1, \qquad (3.23)$$

we have obtained by elimination, solving problems of the form (3.21) with $A = 1$, the quadratic corrections V_2, Ψ_2 and Θ_2, $\widetilde{\Theta}_2$. With the use of the scalar product

$$((\psi, \theta), (\psi_a, \theta_a)) \longmapsto \langle r(\psi \psi_a^* + \theta \theta_a^*) \rangle_{r\varphi}, \qquad (3.24)$$

we have obtained the adjoint problem corresponding to the linearized version of (3.4),

$$i\omega_c(-\Delta \psi_a) - 2E^{-1}H^{-2}\partial_\varphi \psi_a = \Delta(-\Delta \psi_a) - \tfrac{2}{3}Ra_c\partial_\varphi \theta_a$$
$$+ f_E F_A(\psi_a) + \tfrac{1}{6}Ra_c g_E G_A(\theta_a), \quad (3.25a)$$

$$i\omega_c \theta_a = \Delta \theta_a + \partial_\varphi \psi_a, \qquad (3.25b)$$

with ψ_a, of the form $\Psi_a(r)\exp[i(m\varphi - \omega_c t)]$, the adjoint streamfunction, θ_a, of the

$E/2$	$E^{-2/3}\tau_0$	c_0	g	gc_1	c_1
10^{-3}	2.137	-0.553	$+0.178$	-0.140	-0.790
10^{-4}	2.182	-0.711	$+0.231$	-0.155	-0.670
10^{-5}	2.209	-0.672	$+0.371$	-0.257	-0.694
10^{-6}	2.266	-0.680	$+0.558$	-1.066	-1.909
10^{-7}	2.189	-0.645	-4.507	-2.739	$+0.608$

TABLE 4. Coefficients of the Landau equation (2.5) for the QG model. The scaling for τ_0 is inspired from the one for ω_c given by the linear theory of Cole (2004).

form $\Theta_a(r)\exp[i(m\varphi - \omega_c t)]$, the adjoint temperature modulation,

$$F_A(\psi_a) = \partial_r^2\psi_a + \tfrac{1}{2}r^{-1}H^{-2}(3r^2 + 2r_o^2)\partial_r\psi_a$$
$$+ \tfrac{1}{2}r^{-2}H^{-4}\{3r^4 + 2r_o^4\partial_\varphi^2 + r_o r^2[2r_o(2 - \partial_\varphi^2) + 5H\partial_\varphi]\}\psi_a, \quad (3.26a)$$

$$G_A(\theta_a) = \partial_r^2\theta_a + \tfrac{1}{2}r^{-1}H^{-2}(2r_o^2 - 5r^2)\partial_r\theta_a$$
$$+ \tfrac{1}{2}r^{-2}H^{-4}\{r^4 + 2r_o^4\partial_\varphi^2 + r_o r^2[-2r_o(2 + \partial_\varphi^2) + 5H\partial_\varphi]\}\theta_a. \quad (3.26b)$$

Note that in this section we fix $m = m_c$. Provided that the normalization condition

$$\langle r[\zeta(\mathbf{v}_1)\psi_a^* + \theta_1\theta_a^*]\rangle_{r\varphi} = \tau_0 \quad (3.27)$$

is fulfilled, the nonlinear term in (2.5) can be obtained by a projection of the resonant nonlinear terms in (3.4) onto the adjoint mode,

$$g(1 + ic_1) = G_{12}^v + G_{21}^v + g_{12}^v + g_{21}^v + G_{12}^t + G_{21}^t + g_{12}^t + g_{21}^t, \quad (3.28a)$$

with

$$\left.\begin{aligned}
G_{12}^v &= \langle r\mathbf{v}_1 \cdot \nabla\zeta(V_2)\,\psi_a^*\rangle_{r\varphi}, & G_{12}^t &= \langle r\mathbf{v}_1 \cdot \nabla(\Theta_2)\,\theta_a^*\rangle_{r\varphi}, \\
G_{21}^v &= \langle r\mathbf{V}_2 \cdot \nabla\zeta(\mathbf{v}_1)\,\psi_a^*\rangle_{r\varphi}, & G_{21}^t &= \langle r\mathbf{V}_2 \cdot \nabla(\theta_1)\,\theta_a^*\rangle_{r\varphi}, \\
g_{12}^v &= \langle r\mathbf{v}_1^* \cdot \nabla\zeta(\mathbf{v}_2)\,\psi_a^*\rangle_{r\varphi}, & g_{12}^t &= \langle r\mathbf{v}_1^* \cdot \nabla(\theta_2)\,\theta_a^*\rangle_{r\varphi}, \\
g_{21}^v &= \langle r\mathbf{v}_2 \cdot \nabla\zeta(\mathbf{v}_1^*)\,\psi_a^*\rangle_{r\varphi}, & g_{21}^t &= \langle r\mathbf{v}_2 \cdot \nabla(\theta_1^*)\,\theta_a^*\rangle_{r\varphi}.
\end{aligned}\right\} \quad (3.28b)$$

The values of the linear Landau coefficients τ_0 and c_0 obtained by an expansion of the temporal eigenvalue of the linear problem, and of the nonlinear Landau coefficients g and c_1 obtained from (3.28) are given in table 4. Once g is known, the physical value of the amplitude A of a saturated wave is calculated as

$$|A| = \sqrt{\epsilon/g}, \quad (3.29)$$

with $\epsilon = Ra/Ra_c - 1 = 0.01$ in the case of figures 5, 6 and 7. Thus it is possible to compare the convection amplitude predicted by the two-dimensional model,

$$\max v_r^{2D} = 2m|A| = 2m\sqrt{\epsilon/g} \quad (3.30)$$

according to (3.7), (3.23), to the same amplitude predicted numerically by the three-dimensional code. The first part of table 5 confirms the impression given by figures 5(*b*) and 5(*e*), i.e. that the QG model overestimates the strength of the radial flow in the equatorial plane. This effect resembles that noted at the end of §3.4: the QG model 'feels' the fact, visible in figure 5(*c*), that the radial velocity is larger out of

$E/2$	$\max v_r^{3D}$	$\max_{EA} v_r^{3D}$	$\max v_r^{2D}$	$\max v_r^{2D}/\max v_r^{3D}$
10^{-3}	2.04	1.41	1.90	0.93
10^{-4}	3.64	2.54	3.33	0.92
10^{-5}	5.52	4.02	5.26	0.95
$E/2$	$\min V^{3D}$	$\min_{EA} V^{3D}$	$\min V^{2D}$	$\min V^{2D}/\min V^{3D}$
10^{-3}	−0.0591	−0.0591	−0.0417	0.70
10^{-4}	−0.105	−0.105	−0.0904	0.86
10^{-5}	−0.151	−0.151	−0.150	1.00
$E/2$	γ^{3D}		γ^{2D}	γ^{2D}/γ^{3D}
10^{-3}	+1.16		+0.290	+0.25
10^{-4}	+0.469		−0.0387	−0.08
10^{-5}	+0.305		+0.0195	+0.06

TABLE 5. The first two parts show the amplitudes of the saturated critical wave and its mean flow at a distance $\epsilon = 0.01$ from onset, measured either in the whole shell or in the equatorial annulus (EA) in the three-dimensional case. The last part shows the total frequency-shift coefficients defined by (3.31).

the equatorial plane around $r = r_c$. A reassuring result of table 5 is that $\max v_r^{2D}$ approaches $\max v_r^{3D}$ when E decreases. Contrary to the wave flow, the mean flow around $r = r_c$ is weaker out of the equatorial plane (figure 5d), and this partly explains why the QG model underestimates the strength of the mean flow (second part of table 5). Note that the QG model without Ekman pumping, i.e. using $f_E = g_E = 0$, largely overestimates $|\min_r V|$, since for the test values $E/2 = (10^{-3}, 10^{-4}, 10^{-5})$ the corresponding ratios $(0.70, 0.86, 1.00)$ in table 5 change to $(2.21, 2.07, 2.60)$. For completeness, another important nonlinear effect should be mentioned: the fact that the waves slow down significantly in the nonlinear regime. In the three-dimensional model, the nonlinear waves thus exhibit an angular frequency of the form

$$\omega = \omega_c[1 - \gamma\epsilon + O(\epsilon^2)], \tag{3.31}$$

where $\gamma > 0$ is a total frequency-shift coefficient of order 1 (last part of table 5). The weakly nonlinear waves calculated with the QG model also admit a total frequency-shift coefficient

$$\gamma^{2D} = (c_0 - c_1)/(\tau_0\omega_c), \tag{3.32}$$

which describes a competition between linear effects accelerating the waves since $c_0 < 0$ (table 4) and nonlinear effects decelerating the waves since $c_1 < 0$ (for a not too small E). Since c_0 and c_1 are close, their difference is small and changes sign with the Ekman number in the domain $2 \times 10^{-3} \geqslant E \geqslant 2 \times 10^{-5}$ where the coefficient $\gamma^{3D} > 0$. This discrepancy contrasts with the nearly quantitative agreement observed for the flow amplitudes, and illustrates the high sensitivity of these nonlinear calculations.

An interesting prediction of the two-dimensional QG model displayed in table 4, in the regime of very small Ekman numbers out of reach of the three-dimensional code, is that the bifurcation to the thermal Rossby waves becomes subcritical for

$$E \leqslant E_2 = 1.6 \times 10^{-6} \pm 2 \times 10^{-7}. \tag{3.33}$$

This transition, which has been suspected to exist since the pioneering work of Soward (1977), has also been evidenced by Cole (2004) with a different QG model using

$E/2$	$\mathrm{Re}(G^v_{12})$	$\mathrm{Re}(G^v_{21})$	$\mathrm{Re}(G^t_{12})$	$\mathrm{Re}(G^t_{21})$	$\mathrm{Re}(g^v_{12})$	$\mathrm{Re}(g^v_{21})$	$\mathrm{Re}(g^t_{12})$	$\mathrm{Re}(g^t_{21})$
10^{-3}	+0.0081	−0.013	+0.16	+0.014	+0.0076	−0.0058	+0.0021	+0.0026
10^{-4}	+0.010	−0.027	+0.19	+0.049	+0.0091	−0.0045	−0.0011	+0.0050
10^{-5}	+0.017	−0.050	+0.26	+0.14	+0.0070	−0.0030	−0.0014	+0.0041
10^{-6}	+0.067	−0.22	+0.29	+0.41	+0.011	−0.0042	+0.0020	+0.0054
10^{-7}	+0.0039	−0.86	−2.2	−1.5	+0.0053	−0.0002	+0.013	+0.0018

$E/2$	$\mathrm{Im}(G^v_{12})$	$\mathrm{Im}(G^v_{21})$	$\mathrm{Im}(G^t_{12})$	$\mathrm{Im}(G^t_{21})$	$\mathrm{Im}(g^v_{12})$	$\mathrm{Im}(g^v_{21})$	$\mathrm{Im}(g^t_{12})$	$\mathrm{Im}(g^t_{21})$
10^{-3}	+0.0075	−0.0092	−0.10	−0.041	+0.00035	−0.0016	+0.0085	−0.00047
10^{-4}	+0.011	−0.021	−0.10	−0.053	+0.0042	−0.0026	+0.0085	+0.0015
10^{-5}	+0.019	−0.060	−0.16	−0.070	+0.0054	−0.0020	+0.0064	+0.0024
10^{-6}	+0.012	−0.14	−0.60	−0.35	+0.0026	−0.00026	+0.0075	+0.00079
10^{-7}	−0.33	+1.1	−1.1	−2.3	−0.019	+0.0074	−0.0040	−0.0090

TABLE 6. Detail of the contributions to the real and imaginary parts of the nonlinear Landau coefficient $g(1 + ic_1)$ (3.28).

$E/2$	10^{-3}	10^{-4}	10^{-5}	10^{-6}	10^{-7}
$\mathrm{Re}(G^v_{12} + G^v_{21} + G^t_{21})$	+0.0099	+0.032	+0.11	+0.25	−2.3

TABLE 7. Sum of the contributions to g in table 6 that correspond to couplings between the mean flow V_2 and the primary wave.

stress-free boundary conditions, hence without Ekman pumping effects. The radius ratio was also smaller, $\eta = 0.2$. The value of the Ekman number at the codimension-2 point was $\simeq 6 \times 10^{-7}$ of similar magnitude. This subcritical transition appears to be a robust feature of the internal heating models, since it is also observed within a QG model with $\eta = 0.35$, $f_E = g_E = 0$, i.e. neglecting all Ekman pumping effects, for

$$\widetilde{E}_2 = 1.3 \times 10^{-6} \pm 2 \times 10^{-7}.$$

This model corresponds to that of Morin & Dormy (2004), who explored the interval $4.7 \times 10^{-7} \leqslant E \leqslant 4.7 \times 10^{-5}$ in our scaling. They found no direct evidence of a subcritical bifurcation. This might be due to the subcritical range being quite narrow, to numerical problems, or to the action of instabilities that could 'destroy' the subcritical branches (see §4).

In order to analyse the nonlinear effects that control the values of g and c_1, we have created table 6. It shows first that the second harmonic modes v_2 and θ_2 play a minor role in these effects, since the corresponding contributions g^v_{12}, g^v_{21}, g^t_{12} and g^t_{21} are of small magnitude in comparison with the contributions associated with the mean modes V_2 and Θ_2. A second important point is that, although the form of the mean flow V_2 remains similar whatever the Ekman number, except for a localization around $r \simeq r_c$, the contributions of V_2 to g, saturating at not too small an Ekman number, become anti-saturating at very small Ekman number; this is proved more precisely by table 7. A last important point revealed by table 6 is that thermohydrodynamical effects are crucial, since for all the values of E studied, the largest contributions to g or gc_1 are always given either by G^t_{12} or G^t_{21}, which corresponds to advection terms in the heat equation (3.4b). This points to the importance of another mean mode, i.e. the mean temperature mode Θ_2, which intervenes in the coefficient G^t_{12}.

4. Concluding discussion

It should be clear that the formulae (2.6) and (2.10),

$$\tau_{xx} = -2E_{cx}, \quad \tau_{yy} = -2E_{cy}, \quad \tau_{xy} = \tau_{yy}\tan\alpha, \tag{4.1}$$

in the Cartesian case, (3.19) and (3.20),

$$\tau_{rr} = -2E_{cr}, \quad \tau_{\varphi\varphi} = -2E_{c\varphi}, \quad \tau_{r\varphi} = \tau_{rr}\tan\alpha, \tag{4.2}$$

in the cylindrical case, with $\tan\alpha$ the slope of the separatrices (see e.g. figures 4c and 6a), are general and valid for all fluctuating velocity fields assuming the form of a pure wave (2.1) or (3.7). In fact, instances where the dependence on time of the complex wave-streamfunction is no more exponential, e.g.

$$\boldsymbol{v}_1 = (\partial_y\psi_1)\boldsymbol{e}_x - (\partial_x\psi_1)\boldsymbol{e}_y \quad \text{with} \quad \psi_1 = \Psi_1(y, t)\exp(\mathrm{i}qx) \tag{4.3}$$

instead of (2.1b) in the Cartesian case, can also be analysed with our reformulation; now the kinetic energies and the slope depend on time. This applies for instance to a transiently growing wavy perturbation of plane Couette flow, which is linearly stable. Using (4.1) and $U_0(y) = y$, we can write the source term for energy growth in the energy equation (2.12) as

$$\langle\tau_{xy}(y, t)U_0'(y)\rangle_y = -2\langle E_{cy}(y, t)\tan\alpha(y, t)\rangle_y. \tag{4.4}$$

Thus we understand why, in figure 9 of Farrell (1988) showing the development of an optimal perturbation, we start with very negative values of α, whereas the growth stops when α, on average, vanishes. Alternately, our analysis also applies to the case of a very strong instability, as illustrated by §2.5 concerning mixing layers. In fact, in some cases, the nonlinear (spatial) saturation of the mixing-layer instability could be understood in terms of a reorientation of the Kelvin–Helmholtz vortices which would slope 'forward' at a certain distance from the trailing edge. Such effects, described as 'vortex nutations' by some authors, are for instance advocated in the §4.4 of Ho & Huerre (1984). In their figure 21, these authors present a geometrical analysis of this phenomenon which corresponds to our analysis.

   A generalization of the reformulation (4.1), (4.2) to fully three-dimensional waves, though possible in principle, may be too intricate to be useful. The velocity field of a pure incompressible three-dimensional wave depends generally on two complex potentials in a complicated manner; another problem is that it will be generally impossible to define a continuous argument (or phase) of these two potentials in the region of the plane where they are defined (e.g. the cross-section of the pipe for pipe flow), because the potentials typically present some zeros.

   We believe that the results displayed in §3 for rotating shell convection will be useful to the geophysics community. The idea of using reduced two-dimensional models for flow computations coupled to a full three-dimensional solver of the induction equation is now emerging in the field of the geodynamo (see e.g. the kinematic dynamo studies by Schaeffer & Cardin 2006), and therefore it appears important to develop reliable, validated, QG models. From this point of view, the comparisons concerning the wave- and mean-flow amplitudes shown in table 5 constitute the first semi-quantitative 'validation' of a QG model in the nonlinear regime. A weak point, however, is revealed by the discrepancies concerning the total frequency-shift coefficient γ, which are also observed within variants of the QG model (for instance the model which includes Ekman pumping effects on the mean flow only yields $\gamma^{2D} < 0$ for $E/2 = 10^{-3}$ and 10^{-4}).

As mentioned in §3.3, and visible in table 2, the critical parameters of the QG model fit the scaling laws of the asymptotic theory with discrepancies smaller than 17% as soon as $E \leqslant 2 \times 10^{-5}$. On the contrary, to reach an asymptotic regime concerning the weakly nonlinear properties of the waves seems to require extremely low value of E, at least $E < 2 \times 10^{-7}$: this is proved by the fact that the coefficients $\mathrm{Re}(G_{12}^t)$, $\mathrm{Re}(G_{21}^t)$ and $\mathrm{Im}(G_{21}^v)$, for instance, change sign between the two last lines of table 6. This is probably linked to the fact that the phase function of the critical wave converges only very slowly towards its asymptotic form, as revealed by the table 3: for the smallest value of the Ekman number, $E = 2 \times 10^{-7}$, the tilt angle at the critical radius is still 19% smaller than its asymptotic value. It would be interesting to develop a weakly nonlinear theory of the thermal Rossby waves valid asymptotically in the limit $E \to 0$, but obviously much effort will be required to validate this theory numerically.

One should be aware that, at finite values of E, the thermal Rossby waves are typically subject to a secondary vacillation instability at rather small values of ϵ, as shown, for instance, by the numerical simulations of Tilgner & Busse (1997) with a three-dimensional model, and by Cole (2004), Morin & Dormy (2004) with cylindrical QG models. Morin & Dormy noted that the critical value of ϵ required to set the vacillation instability becomes quite small when E diminishes, and that the vacillation instability then transforms into a pulsed instability leading to relaxation oscillations (like the ones shown in the figure 8 of Morin & Dormy 2004). It would be interesting to run new simulations of this kind in a clearly subcritical case. We can conjecture that the subcritical waves will always be unstable, but the exact behaviour of the system has still to be established. It might be that instabilities always drive the system back to the conduction state, i.e. that, effectively, subcritical convection will be difficult to observe.

It is difficult to propose a physical interpretation of the nonlinear properties of these rotating convection models, even in the framework of the QG weakly nonlinear analysis. For instance the simplest nonlinear coefficient appearing in this analysis is

$$G_{21}^t = \langle r \boldsymbol{V}_2 \cdot \boldsymbol{\nabla}(\theta_1)\theta_a^* \rangle_{r\varphi} = \mathrm{i}m \langle V_2 \Theta_1 \Theta_a^* \rangle_r , \tag{4.5}$$

which involves the phase functions of Θ_1 and Θ_a. These functions vary significantly in the annulus because of the spiralling character of the waves. As a result, the integrand in (4.5) is oscillating and it is difficult to explain the sign of the real and imaginary parts of this integral. It will be interesting to study in the same way the case of differential heating models, when there are no heat sources in the fluid, and consequently the convection attaches to the inner radius. A conjecture made by Gillet & Jones (2006) (see their §3.1) is that, since the distinction between the local and global asymptotic theories is then lost, the first bifurcation should stay supercritical. That should be verified.

Appendix. The slope of the separatrices is the average slope of the streamlines

For x, y waves, Pedlosky (1987) offered a local formula where the 'inverse' slope of the streamline passing through the point under consideration intervenes,

$$-v_x v_y = (\partial_y \psi)(\partial_x \psi) = -(\partial_y \psi)^2 y_\psi'(x) = -v_x^2 y_\psi'(x), \tag{A 1}$$

$y_\psi(x)$ designating locally the parameterization of this streamline. Yet we know now that, when the average over x is applied, it is the slope $x'_s(y)$ of the separatrices, which are special cases of streamlines, that comes in. A connection can, however, be made between our formula (2.10) and the approach of Pedlosky (1987). For this we write locally

$$-v_x v_y = (\partial_y \psi)(\partial_x \psi) = -(\partial_x \psi)^2 x'_\psi(y) = -v_y^2 x'_\psi(y),$$ (A 2)

$x_\psi(y)$ being another parameterization of the streamline. It happens that, when the average over x is applied, for pure wave-flows v of the form (2.1),

$$\tau_{xy} = -\langle v_x v_y \rangle_x = -\langle v_y^2 \rangle_x \langle x'_\psi(y) \rangle_x,$$ (A 3)

i.e. the average slope of the streamlines is the slope of the separatrices,

$$\langle x'_\psi(y) \rangle_x = x'_s(y)$$ (A 4)

with the notation of §2.3. This formula can be established as follows: denoting $\rho(y) = |\Psi_1(y)|$ and $\phi(y) = \arg[\Psi_1(y)] + \arg(A) - \omega t$, we can check that locally

$$x'_\psi(y) = -\frac{\partial_y \psi}{\partial_x \psi} = \frac{\rho'(y)}{q\rho(y)} \cotan[qx + \phi(y)] - \frac{\phi'(y)}{q}.$$

The first term, which is oscillating, presents a vanishing average; the second term is $x'_s(y)$.

When a mean flow $V_0 = U_0(y)e_x$ is added to the pure wave, i.e. the flow $V_0 + v$ corresponding to the total streamfunction

$$\psi = \int_{y_0}^y U_0(Y)\,dY + 2|A|\rho(y)\cos[qx + \phi(y)]$$

is examined, we finds locally for the slope of a streamline

$$x'_\psi(y) = \frac{U_0(y)}{2|A|q\rho(y)\sin[qx + \phi(y)]} + \frac{\rho'(y)}{q\rho(y)}\cotan[qx + \phi(y)] - \frac{\phi'(y)}{q}.$$

Consequently, we still has (A 4); this property is used in §2.5.

The same properties hold for waves in cylindrical geometry, given by (3.7), i.e. if $\varphi_\psi(r)$ designates locally the parameterization of the streamlines of a pure wave to which a mean flow can be added,

$$\langle r\varphi'_\psi(r) \rangle_\varphi = r\varphi'_s(r)$$ (A 5)

with the notation of §3.4.1.

REFERENCES

AUBERT, J., GILLET, N. & CARDIN, P. 2003 Quasigeostrophic models of convection in rotating spherical shells. *Geochem. Geophys. Geosyst.* **4**, 1052–1–19.

AURNOU, J. M. & OLSON, P. L. 2001 Strong zonal winds from thermal convection in a rotating spherical shell. *Geophys. Res. Lett.* **28**, 2557–2560.

BUSSE, F. H. 1970 Thermal instabilities in rapidly rotating systems. *J. Fluid Mech.* **44**, 441–460.

BUSSE, F. H. 1983 Generation of mean flows by thermal convection. *Physica* D **9**, 287–299.

BUSSE, F. H. 2002 Convective flows in rapidly rotating spheres and their dynamo action. *Phys. Fluids* **14**, 1301–1314.

BUSSE, F. H. & CARRIGAN, C. R. 1983 An experimental and theoretical investigation of the onset of convection in rotating spherical shells. *J. Fluid Mech.* **126**, 287–305.

BUSSE, F. H. & HOOD, L. L. 1982 Differential rotation driven by convection in a rapidly rotating annulus. *Geophys. Astrophys. Fluid Dyn.* **21**, 59–74.

BUSSE, F. H. & OR, A. C. 1986 Convection in a rotating cylindrical annulus: thermal Rossby waves. *J. Fluid Mech.* **166**, 173–187.

CHRISTENSEN, U. R. 2002 Zonal flow driven by strongly supercritical convection in rotating spherical shells. *J. Fluid Mech.* **470**, 115–133.

CHRISTENSEN, U. R., AUBERT, J., CARDIN, P., DORMY, E., GIBBONS, S., GLATZMAIER, G. A., GROTE, E., HONKURA, Y., JONES, C., KONO, M., MATSUSHIMA, M., SAKURABA, A., TAKAHASHI, F., TILGNER, A., WICHT, J. & ZHANG, K. 2001 A numerical dynamo benchmark. *Phys. Earth Planet. Inter.* **128**, 25–34.

COLE, S. 2004 Nonlinear rapidly rotating spherical convection. PhD thesis, University of Exeter, http://www.maths.leeds.ac.uk/~cajones/cole.html.

CORCOS, G. M. & SHERMAN, F. S. 1984 The mixing layer: deterministic model of a turbulent flow. Part 1. Introduction and the two-dimensional flow. *J. Fluid Mech.* **139**, 29–65.

DORMY, E., SOWARD, A. M., JONES, C. A., JAULT, D. & CARDIN, P. 2004 The onset of thermal convection in rotating spherical shells. *J. Fluid Mech.* **501**, 43–70.

FARRELL, B. F. 1988 Optimal excitation of perturbations in viscous shear flow. *Phys. Fluids* **31**, 2093–2102.

FUJIMURA, K. 1987 Landau constant of plane Poiseuille flow near the neutral state. *Phys. Fluids* **30**, 1216–1218.

GILLET, N. & JONES, C. A. 2006 The quasi-geostrophic model for rapidly rotating spherical convection outside the tangent cylinder. *J. Fluid Mech.* **554**, 343–369.

GILLET, N., BRITO, D., JAULT, D. & NATAF, H.-C. 2007 Experimental and numerical studies of convection in a rapidly rotating spherical shell. *J. Fluid Mech.* **580**, 83–121.

HERBERT, T. 1980 Nonlinear stability of parallel flows by high-order amplitude expansions. *AIAA J.* **18**, 243–248.

HO, C. M. & HUERRE, P. 1984 Perturbed free shear layers. *Annu. Rev. Fluid Mech.* **16**, 365–424.

HUERRE, P. & ROSSI, M. 1998 Hydrodynamic instabilities in open flows. *Hydrodynamics and Nonlinear Instabilities* (ed. C. Godrèche & P. Manneville), pp. 81–294. Cambridge University Press.

JONES, C. A., SOWARD, A. M. & MUSSA, A. I. 2000 The onset of thermal convection in a rapidly rotating sphere. *J. Fluid Mech.* **405**, 157–179.

KAGEYAMA, A. & SATO, T. 1997 Generation mechanism of a dipole field by a magnetohydrodynamic dynamo. *Phys. Rev. E* **55**, 4617–4626.

MICHALKE, A. 1964 On the inviscid instability of the hyperbolic-tangent velocity profile. *J. Fluid Mech.* **19**, 543–556.

MORIN, V. & DORMY, E. 2004 Time dependent β-convection in rapidly rotating spherical shells. *Phys. Fluids* **16**, 1603–1609.

MORIN, V. & DORMY, E. 2006 Dissipation mechanisms for convection in rapidly rotating spheres and the formation of banded structures. *Phys. Fluids* **18**, 068104–1–4.

PEDLOSKY, J. 1987 *Geophysical Fluid Dynamics*. Springer.

PLAUT, E. 2003 Nonlinear dynamics of traveling waves in rotating Rayleigh–Bénard convection: effects of the boundary conditions and of the topology. *Phys. Rev. E* **67**, 046303, 1–11.

PLAUT, E. & BUSSE, F. H. 2002 Low-Prandtl-number convection in a rotating cylindrical annulus. *J. Fluid Mech.* **464**, 345–363.

PLAUT, E. & BUSSE, F. H. 2005 Multicellular convection in rotating annuli. *J. Fluid Mech.* **528**, 119–133.

PROCTOR, M. R. E. 1994 Convection and magnetoconvection in a rapidly rotating sphere. *Lectures on Solar and Planetary Dynamos* (ed. M. R. E. Proctor & A. D. Gilbert), pp. 97–115. Cambridge University Press.

REYNOLDS, O. 1895 On the dynamical theory of incompressible viscous fluids and the determination of the criterion. *Phil. Trans. R. Soc. Lond.* **186**, 123–164.

REYNOLDS, W. C. & POTTER, M. C. 1967 Finite-amplitude instability of parallel shear flows. *J. Fluid Mech.* **27**, 465–492.

SCHAEFFER, N. & CARDIN, P. 2005 Quasigeostrophic model of the instabilities of the Stewartson layer in flat and depth-varying containers. *Phys. Fluids* **17**, 104111–1–12.

SCHAEFFER, N. & CARDIN, P. 2006 Quasi-geostrophic kinematic dynamos at low magnetic Prandtl number. *Earth Planet. Sci. Lett.* **245**, 595–604.

SCHMID, P. J. & HENNINGSON, D. S. 2001 *Stability and Transition in Shear Flows*. Springer.

SIMITEV, R. & BUSSE, F. H. 2003 Patterns of convection in rotating spherical shells. *New J. Phys.* **5**, 97–1–20.

SIMITEV, R. & BUSSE, F. H. 2005 Prandtl-number dependence of convection-driven dynamos in rotating spherical fluid shells. *J. Fluid Mech.* **532**, 365–388.

SOWARD, A. M. 1977 On the finite amplitude thermal instability of a rapidly rotating fluid sphere. *Geophys. Astrophys. Fluid Dyn.* **9**, 19–74.

TILGNER, A. & BUSSE, F. H. 1997 Finite-amplitude convection in rotating spherical fluid shells. *J. Fluid Mech.* **332**, 359–376.

ZHANG, K. 1992 Spiralling columnar convection in rapidly rotating spherical fluid shells. *J. Fluid Mech.* **236**, 535–556.